Optical properties and ferroelectric engineering of vapor-transport-equilibrated, near-stoichiometric lithium tantalate for frequency conversion

D. S. Hum,[a] R. K. Route, G. D. Miller, V. Kondilenko, A. Alexandrovski, J. Huang, K. Urbanek, R. L. Byer, and M. M. Fejer
E.L. Ginzton Laboratory, Stanford University, Stanford, California 94305-4088

(Received 19 July 2006; accepted 2 March 2007; published online 9 May 2007)

Near-stoichiometric lithium tantalate (SLT) crystals were produced from congruent lithium tantalate by vapor transport equilibration, and several important optical and ferroelectric properties were measured. The effect of vapor transport conditions and surface preparation on reproducible ferroelectric engineering of SLT has been studied. Control of these effects along with dramatic decreases in the sensitivity to photorefractive damage and 532 nm absorption has allowed near-room-temperature generation of 10 W of continuous wave 532 nm radiation by second harmonic generation from 29 W of 1064 nm radiation in a 4 cm long device. © *2007 American Institute of Physics*. [DOI: 10.1063/1.2723867]

I. INTRODUCTION

Frequency conversion using quasi-phase-matched nonlinear devices is efficient and engineerable. One method of quasi-phase-matching can be realized by periodically poling ferroelectrics. Periodically poled lithium niobate ($LiNbO_3$, LN) has been perhaps the most popular of these ferroelectrics because of its high nonlinearity and the availability of high optical quality substrates. Commonly available, congruent-composition lithium niobate, like many ferroelectrics, is limited in applications involving visible light by photorefractive damage (PRD)[1] and by green-induced infrared absorption (GRIIRA).[2] Lithium tantalate ($LiTaO_3$, LT), a widely used isomorph of lithium niobate, suffers similar limitations.

Recently, studies of the mechanisms responsible for these effects suggest that the material limitations arise from intrinsic defects in the congruently grown crystals, which are ~1.5% lithium deficient. Melt-grown near-stoichiometric crystals have been shown to be less susceptible to PRD and GRIIRA,[1,3] and are viable candidates for efficient frequency conversion.[4,5] However, techniques that produce near-stoichiometric crystals from a melt are technically challenging.[6]

The vapor-transport-equilibration (VTE) method provides an alternative to direct melt-growth techniques to produce crystals of various compositions including near-stoichiometric crystals.[7] Near-stoichiometric crystals have been shown to have dramatically reduced intrinsic defect concentrations, and dramatically reduced susceptibility to PRD.[8] This has enabled the demonstration of efficient and stable frequency conversion at high average and high peak powers at near-room temperature.[9] In this article, we describe the effects of VTE on important optical and ferroelectric properties of LT, and their impact on domain engineering for frequency conversion applications.

[a]Corresponding author; electronic mail: dhum@stanford.edu

II. BACKGROUND

Crystals of lithium tantalate can exist over a wide range of compositions, from approximately 47 mol % lithium oxide to approximately 50 mol % lithium oxide. Many physical properties of lithium tantalate depend strongly on crystal composition.[10] Properties such as Curie temperature, birefringence, NMR spectra, and Raman spectra are dependent on composition. Most commercially available lithium tantalate is grown from melts of the congruently melting composition, 48.39 mol % lithium oxide (Li_2O), and this produces crystals of the same composition with a Curie temperature of 605.3 °C.[11] In comparison, crystals of near-stoichiometric composition, 49.95 mol % lithium oxide (Li_2O) with a Curie temperature of 695 °C, are grown from melts with a substantial excess of lithium oxide, with composition on the order of 58 mol % lithium oxide.[6] The defects associated with the lithium deficiency of congruently melting composition are widely accepted to be one Ta^{4+} antisite defect $(Ta_{Li^+}^{5+})^{4+}$ plus an additional four lithium vacancies nearby which are required for charge neutrality.[12] The concentration of antisite Ta^{4+} intrinsic defects closely correlates with the magnitude of PRD and GRIIRA[9] under the high optical intensities typical of frequency conversion applications. Defect studies by others have led to the polaron/bipolaron model for the Ta^{4+} defect, which accounts reasonably well for the absorption bands in congruent lithium tantalate, and it provides a plausible mechanism for carrier excitation and trapping and the resultant optical properties seen in this material.[13] While the Ta^{4+} antisite defect is the source of PRD and GRIIRA, the departure from stoichiometry is usually designated by specifying the lithium content of the crystal.

Due to the strong compositional dependence of PRD and GRIIRA, an accurate measure of the deviation from stoichiometry is essential for predicting device performance in this material. Recently, the ferroelectric coercive field of lithium tantalate has been shown to be a sensitive measure of crystal composition.[14] Measurements suggest that the ferroelectric

coercive field is linearly proportional to the lithium deficiency, ranging from 21 kV/mm in congruently melting lithium tantalate (~1.61 mol % lithium deficient) to 0.1 kV/mm at a near-stoichiometric lithium tantalate (estimated to be ~0.008 mol % lithium deficient).[14]

Ferroelectricity in lithium tantalate was first described by Matthias and Remeika in 1949.[15] Early work in the growth of lithium tantalate characterized crystal composition by measuring the Curie temperature.[16,17] In particular, Ballman *et al.* report Curie temperatures as high as 690 °C via growth from lithium-oxide-rich melts.[17] Measurements of the Curie temperature of ceramic samples suggest that the composition of crystals with that Curie temperature corresponds to a composition in the range 49.9–50.0 mol % Li_2O. These crystals were apparently the first near-stoichiometric lithium tantalate (SLT) crystals grown, but they suffered, as is generally the case for Czochralski growth of compositions far from congruency, from significant inhomogeneity and poor yield. Thus, most manufacturers have chosen to grow congruently melting crystals which provide homogeneous crystals and result in extremely good yield.[11]

Recently, techniques such as the double-crucible, melt-replenishment Czochralski method have produced high-quality SLT crystals with Curie temperatures as high as 695 °C and coercive fields as low as 800 V/mm.[12] These self-flux techniques require precise control of the temperature and material feed rates to ensure homogeneous results. SLT produced in this manner has improved characteristics for frequency conversion applications, including reduced photorefraction,[1] reduced susceptibility to GRIIRA,[2] and improved thermal conductivity.[5] Measurements of ferroelectric coercive field suggest that these techniques have achieved compositions close to 49.95 mol % Li_2O.[12]

As an alternative to direct melt-growth methods, the VTE method can be used to convert commercially available congruently grown crystals into crystals of a desired composition.[18] By heating the sample crystal with an appropriate composition of powder in a loosely sealed system, crystals of nearly any composition that falls within the single-phase $LiTaO_3$ existence region can be produced. In the case of lithium tantalate, Li_2O is exchanged between the single crystal and the powder by vapor transport until equilibrium is achieved. For low photorefractivity and GRIIRA, it is desirable to produce compositions that are very near 50 mol % Li_2O, which lies close to the boundary of the single-phase $LiTaO_3$ existence region, adjacent to the $LiTaO_3+Li_3TaO_4$, two-phase existence region. The vapor pressure of Li_2O for all compositions within the two-phase field is a function only of temperature and does not depend on the specific composition. Thus, powders within the two-phase region can serve as an "infinite" reservoir of Li_2O which can be used to bring the composition of crystals lying within the single-phase existence region, as congruent composition crystals do, to the boundary of the single-phase $LiTaO_3$ existence region, which is very close to the stoichiometric composition. The resultant stoichiometric composition crystal is in phase equilibrium with the two-phase powder, and mass transport of Li_2O stops at this point without the formation of Li_3TaO_4 on the surface. The approach to the stoichiometric composition is an asymptotic process that requires extended processing at high temperatures. It is self-stabilizing, however, and as long as the composition of the powder remains in the two-phase region, i.e., lithium-rich, this process results in a vapor-transport-equilibrated, near-stoichiometric lithium tantalate (VLT) crystal whose composition closely approaches the phase boundary of the single-phase $LiTaO_3$ existence region. The final composition of the resultant crystals is only dependent on the temperature and duration of the VTE process. Using this method, coercive fields as low as 100 V/mm have been achieved, which suggests that the crystal reached a composition of >49.99 mol % Li_2O.[14]

III. CRYSTAL FABRICATION

Optical-grade, z-cut, congruent lithium tantalate (CLT) wafers from Yamaju Ceramics, Inc. were used as the substrate for our VTE experiments. Full 2 inch, one-quarter, and one-sixth wafers with thicknesses of 0.5 and 1 mm were processed. A prereacted mixture of Li_2O (60 mol %) and Ta_2O_5 (40 mol %) powder was produced from appropriate amounts of Li_2CO_3 and Ta_2O_5 to form a two-phase mixture of $LiTaO_3$ and Li_3TaO_4 which served as the source of Li_2O for the VTE process. The congruent-composition wafers were placed in a platinum crucible, standing vertically in a simple platinum wafer holder. A second platinum crucible with a slightly smaller diameter than the first was then placed over the wafer assembly with the rim resting on the presintered powder. The size of the cover crucible was chosen to minimize the area of the presynthesized powder that was exposed to the air. Since Li_2O is slowly volatilized during the VTE process and lost to the environment, the use of a large cover is thought to provide a loose seal by which the vapor pressure of Li_2O can be controlled by the Li_2O equilibrium partial pressure over the two-phase powder. The entire assembly was then heated in a two-temperature process, first to 1360 °C and then 1100 °C in a dry, mostly nitrogen ambient for various lengths of time. After processing, the crucible and the wafers were weighed to determine Li_2O loss and the powder was replaced when the excess Li_2O was depleted, as determined by the weight-loss measurements.

After the VTE process, the VLT crystals had to be uniformly poled before reproducible periodic poling was possible. The uniform poling process was performed at 185 °C with graphite electrodes and applied fields as high as 1000 V/mm to remove the head-to-head domains that result from the VTE process. To ensure complete polarization, the applied field was reversed several times. Afterwards, the crystals were annealed in air at 620 °C for 10 h. We refer to these processed crystals as virgin samples. In reference to their ferroelectric properties, forward poling will refer to the first domain reversal after uniform poling; backward poling will refer to domain reversal back to the original state. The influence of the VTE method on important optical characteristics, domain engineering, and nonlinear device performance on VLT, which have not been discussed previously, are the subject of the remainder of this article.

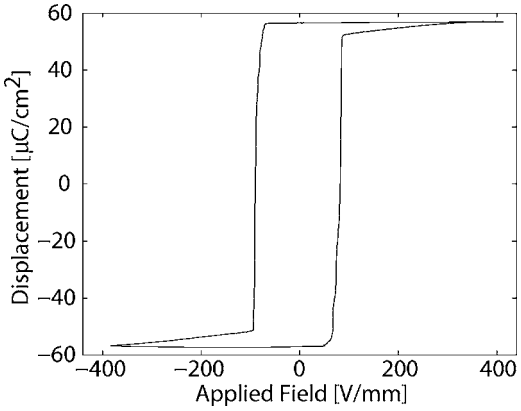

FIG. 1. A typical hysteresis loop for a 9.5 mm diameter area on a 1 mm thick VLT sample with a loop period of 500 s.

IV. FERROELECTRIC PROPERTIES AND DOMAIN ENGINEERING

The ferroelectric properties of VLT are distinctly different from SLT fabricated by melt-growth methods. For example, Gopalan *et al.* show that the coercive field has a linear relationship with the deviation from stoichiometry.[12,14] Thus, a careful study of how VTE affects the ferroelectric properties of the resulting VLT is useful. To engineer an appropriate periodic structure for optical frequency converters, accurate measurements of the coercive field, spontaneous polarization, and domain wall velocity and nucleation as a function of applied electric field are extremely important.[19]

A. Coercive field

Measurements of coercive field and spontaneous polarization were performed on various virgin VLT crystals. Using liquid-electrolyte electrodes contacting a 9.5 mm diameter area, simple hysteresis loops were used to measure these characteristics. A triangle wave with peak-to-peak amplitude of 200 V (or 400 V for coercive fields greater than 200 V) was applied to the crystal with a Trek 623B high voltage amplifier; the current delivered to the sample was measured with a series resistor. The delivered charge, obtained by integrating the measured current, is proportional to the reversed spontaneous polarization over the poled area. If the material being poled is of homogeneous composition, and the magnitude of the spontaneous polarization is uniform, the delivered charge is twice the spontaneous polarization times the poled area, $q(t)=2P_sA(t)$, allowing the spontaneous polarization to be calculated from the charge delivered and the area of the electrode. The spontaneous polarization can be calculated by taking the maximum delivered charge divided by twice the area of the electrode. One can then construct a hysteresis loop of displacement as a function of applied field. A typical hysteresis loop performed on a 1 mm thick sample with a period of 500 s is shown in Fig. 1.

In this work the "apparent" coercive field for both forward and reverse poling is defined as the applied field where the displacement crosses through zero. However, difficulties arise when measuring coercive field, due to the time-dependent nature of poling. To clarify this point, measurements of apparent coercive field as a function of triangle wave period are shown in Fig. 2. These measurements were performed on the same sample area. Since nucleation and domain wall velocity are both field and time dependent, long poling periods result in small coercive fields. However, as the measurement time approaches 1000 s the coercive field approaches an asymptotic value. For convenience, a period of 500 s was selected as a standard measurement time.

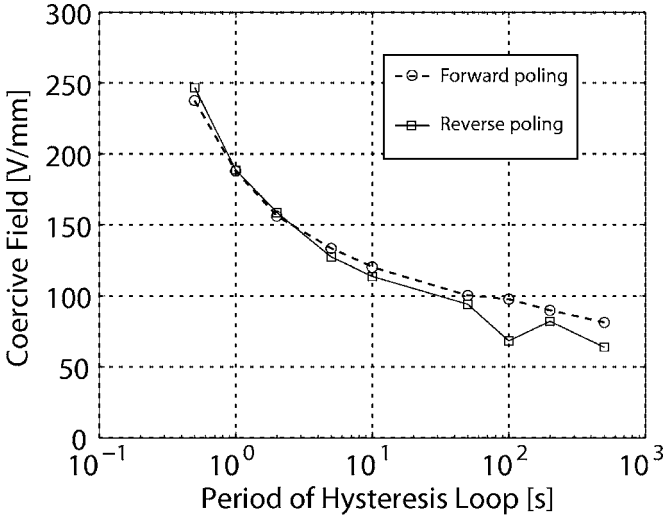

FIG. 2. A typical dependence of coercive field for a single area (9.5 mm diameter) on a 1 mm thick VLT sample as a function of loop period for both forward (circles) and reverse (squares) coercive fields.

To explore the effect of VTE on coercive field and spontaneous polarization, hysteresis loops were measured on several samples, as well as on different locations on some of the samples. Figure 3 shows the measured coercive field as a function of VTE processing time at 1360 °C on samples of two thicknesses, 0.5 and 1.0 mm. Samples treated at 1360 °C and subsequently processed for varying times at 1100 °C showed no significant change in coercive field. It is important to note a few key characteristics appearing in Fig. 3. First, with increasing VTE time the coercive field drops to as low as 60 V/mm. Second, the required VTE time to reach

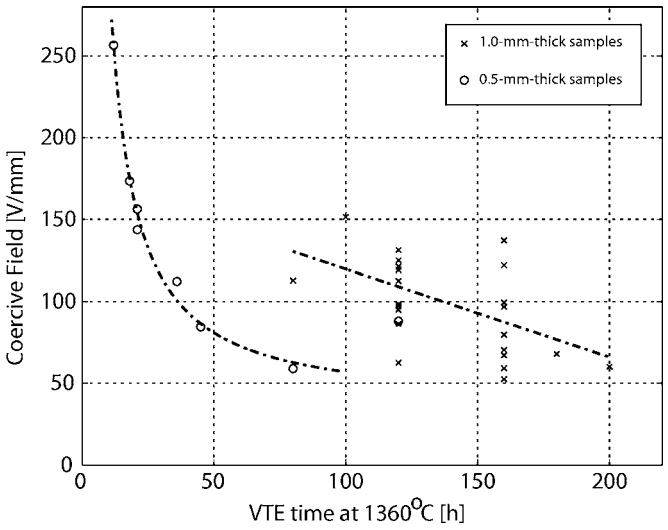

FIG. 3. Coercive field as a function VTE time at 1360 °C. Circles indicate 0.5 mm thick samples and crosses indicate 1 mm thick samples.

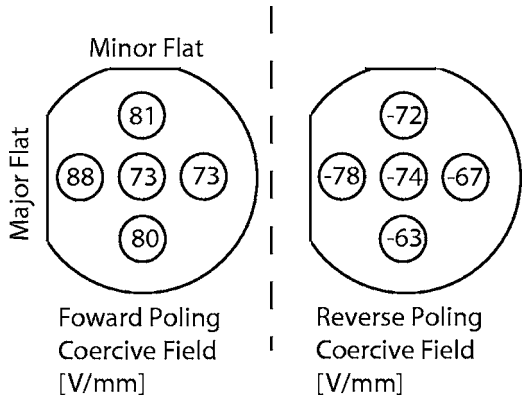

FIG. 4. Coercive field uniformity over a typical wafer.

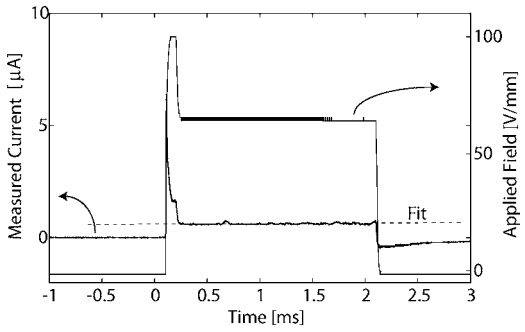

FIG. 5. Voltage and current traces for a typical domain wall velocity measurement.

60 V/mm does not scale with the square of the material thickness, which suggests that the VTE process is not diffusion limited but rather either surface-reaction-rate limited or effusion limited. Material-loss measurements suggest that the two-phase powder, used as the source of Li_2O, sources more than three times the required Li_2O to exchange the original CLT substrates to the stoichiometric composition. Since the covering platinum crucible covers most of the powder area, surface reaction rate is most likely the limiting rate for the VTE process. This surface reaction rate may be important for designing a process to scale to thicker substrates. Assuming that the linear relation between coercive field and deviation from stoichiometry can be extrapolated to these low fields,[12] the reduction in coercive field to 60 V/mm suggests that the VLT crystals are 350 times closer to stoichiometry than their congruently melting counterparts. Given the 48.39 mol % composition of CLT crystals, the VLT crystals correspond to a lithium deficiency of approximately 50 ppm. The asymptotic behavior of the coercive field for long processing times suggests that the $LiTaO_3$ phase boundary is extremely close to 49.996 mol %, corresponding to approximately 50 V/mm, and that it may not be beneficial to VTE to much longer times than are used here.

It is also important to measure the uniformity of 2 inch wafer substrates, as domain engineering and any nonlinear devices will depend critically on the homogeneity of the sample across such a large area.[20] A 9.5 mm diameter O-ring was used to sample five spots on the wafer to test the coercive-field uniformity. Figure 4 shows results in a typical wafer. There is approximately a 15 V/mm difference from one side of the wafer to another. This difference correlates with the orientation of the wafer inside the platinum crucible, with the side of the wafer closest to the powder having a higher coercive field than the side farthest from the powder. Most wafers have been processed with the major flat, i.e., the $+Y$ axis, closest to the powder for ease of mounting the crystals in the crucible. We have not seen any dependence of periodic-poling quality or nonlinear optical performance that could be related to this level of nonuniformity.

B. Domain wall velocity

To understand how the VTE process affects the poling dynamics, attempts to characterize the domain wall velocity versus applied field were performed. Using uniform LiCl electrodes, a poling pulse as shown in Fig. 5 was applied to several samples. A 100 μs nucleation pulse (approximately twice the coercive field) followed by a measurement field of varying times was applied to each sample, and the current delivered to the sample was measured using a series resistor. During the application of measurement field, the current rises linearly if the domain wall velocity is constant assuming isotropic two-dimensional growth. Here, the relative domain wall velocity has been calculated by assuming that the best fit of the rate of change of the measured current at a fixed applied voltage was proportional to the domain wall velocity. It has been shown that the domain wall velocity can increase by orders of magnitude during domain merging.[12] Effects of merging were avoided as only a small fraction of each sample was poled. Figure 6 shows measurements of the relative domain wall velocity for several samples. Since samples of varying coercive fields (E_c, ranging from 70–115 V/mm, approximately 0.7–1.3 times the coercive field) were measured, we have plotted the domain wall velocity against difference of the applied field (E_{app}) and the measured sample coercive field.

The relative domain-wall-velocity measurements show agreement from sample to sample. It is clear that absolute domain wall velocity measurements must be done by measuring real domains inside the poled area. Previous studies

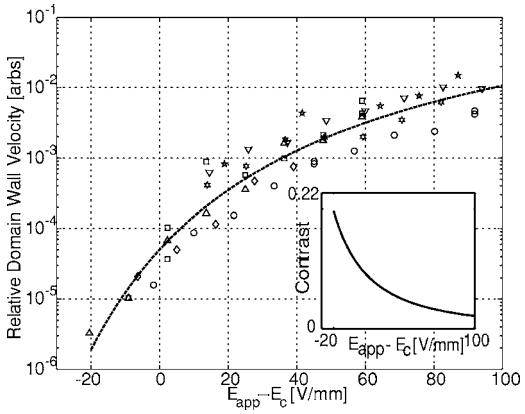

FIG. 6. Relative domain wall velocity measurements as a function of the difference applied field and coercive field. Measurements were performed on several samples with varying coercive fields. (Inset) Contrast (derivative of the log of the domain wall velocity with respect to field) vs the difference of applied field and coercive field.

have used chemical etching to reveal the domains.[19] This visualization method can alter the domain pattern after poling, especially for low coercivity materials like VLT.[21] From these measurements, a fit to these data points shows the following dependence of velocity versus field given in V/mm:

$$v \propto \exp\left(\frac{-750 \pm 130}{E_{\text{app}} - E_c + 78 \pm 9}\right) \quad (1)$$

The bulk of the uncertainty of this fit stems from the sample-to-sample variation of the measured coercive field. This velocity-field curve provides insight into the optimal poling conditions for the material. A contrast curve (the derivative of the of the log of the velocity with respect to applied field, inset in Fig. 6) quantitatively shows the sensitivity of the domain wall velocity to applied field.[19,22] For periodic poling, one would like to operate at the maximum contrast point since it provides the maximum control over the size of poled domains. These measurements suggest using smaller poling fields for maximum contrast. From Refs. 19 and 22, a 1 kV/mm change of electric field provided a contrast value of 5, and this contrast value was required for good periodic poling in magnesium-oxide-doped lithium niobate and congruent niobate, respectively. The charge required to screen the 1 kV/mm electric field results in micron-scale growth of domains underneath the patterned dielectric layer (e.g., patterned photoresist, or patterned spin-on-glass). In VLT, at fields which have good nucleation (approximately 80 V/mm above E_c), for a contrast value of 5, approximately 100 V/mm of electric field is required. Thus, the growth of domains underneath the patterned dielectric layer should be reduced from the order of microns in congruent lithium niobate to tenths of microns in VLT.

C. Domain stability and backswitching

In both lithium niobate and lithium tantalate, after domain reversal one can observe a spontaneous relaxation back to the initial domain state.[23] This phenomenon of spontaneous relaxation is commonly referred to as backswitching and can depend on the ferroelectric, material composition, and temperature. Backswitching can be hindered or enhanced by appropriate choice of the applied poling field. For example, application of stabilization field of 18 kV/mm after poling congruent lithium niobate for only 50 ms will prevent backswitching.

A measurement of the necessary stabilization field can be performed by appropriately manipulating the applied voltage.[24] The applied voltage waveform is shown in Fig. 7. Here, we apply a forward poling pulse and then apply a holding voltage for various times. By measuring the field required to backswitch the poled area as a function of a holding voltage and holding time after poling, one can estimate the hold voltage and time necessary to prevent significant backswitching. A small 9.5 mm diameter area of virgin substrate was forward poled. After a short poling time, a holding voltage was applied for varying times. Once the prescribed hold time was completed, the applied field was ramped toward the reverse coercive field. The backswitching field was measured as the field where the backswitching current rises

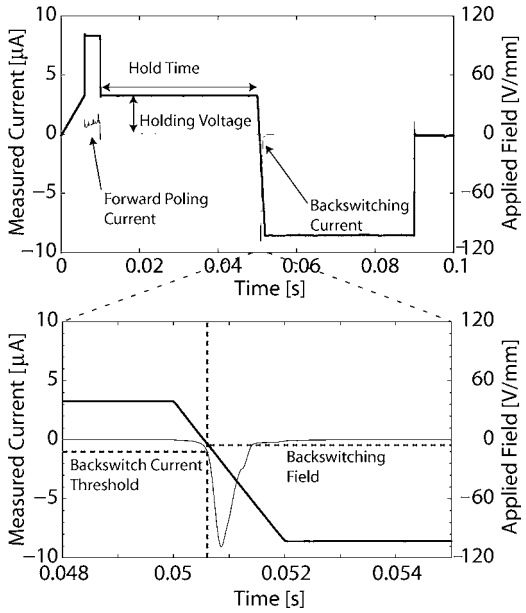

FIG. 7. Voltage and current vs time for a typical backswitching measurement.

above the noise floor (here referred to as the backswitching current threshold). A plot of the dependence backswitching field on hold time and hold voltage is shown in Fig. 8.

The picture drawn from the data is as follows. Immediately after poling, there is a time constant on the order of 100 ms during which the sample is likely to backswitch without a holding voltage. After this time, the backswitching voltage saturates at a value of approximately −11 V/mm. If the applied field reaches this value domain walls can move, causing the existing domains to shrink. If the applied field is too great during this holding period, the sample can completely overpole, at which point the backswitching field becomes the reverse coercive field of the sample. These two levels for backswitching suggest that there is an inherent difference between the field required for domain motion and the field required for domain nucleation. Clearly, with the appropriate choice of holding field and holding time, one would hope to find an operating point to prevent backswitching, stabilize the domains, and not overpole the sample. For samples of

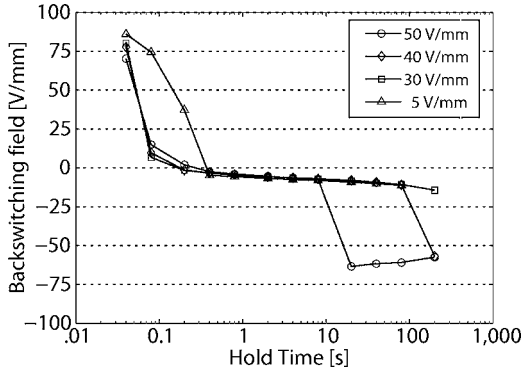

FIG. 8. Backswitching field as a function of hold time for various hold voltages applied to a 1 mm thick sample. Backswitching field is pinned to a level of −11 V/mmuntil the area fully poles and becomes the coercive field. This suggests a difference between domain motion and nucleation fields for long holding times.

different coercive fields, the domain wall velocity will be different for the same stabilization field and thus there is no simple formula for the appropriate choice of stabilization field and time as a function of coercive field. However, we have found for coercive fields close to 100 V/mm, a stabilization field of 55 V/mm for 1 h is sufficient to stabilize the domains with out significant growth of periodically poled domains.

Recently, it has been shown that domains in near-stoichiometric lithium tantalate can rearrange during chemical etching.[21] This domain rearrangement remains a difficult problem to solve in the development of a full process. Periodically poled domains collapse and merge with other nearby domains during the etching with hydrofluoric acid (HF) usually used to reveal the domain structure. This step is not necessary, however, since alternative methods for visualizing the domains can be used to monitor the results of this process. Moreover, polishing before poling, which may be important for adequate lithography, increases this instability. It was found that chemical etching with HF before poling reduces the sensitivity to chemical etching after poling. However, etching prior to periodic poling also alters the poling characteristics of the sample, e.g., too long an etch results in samples susceptible to overpoling. This result suggests that a thin layer at the surface of the as-VTE'ed or as-single-domain-poled sample stabilizes domains and prevents overpoling. Periodically poled domains become unpinned when this layer is chemically removed and they become free to collapse and merge.

D. Domain patterning

Domain backswitching and instabilities during chemical etching have not prevented periodic poling of full 2 inch wafers of high quality. Taking virgin full wafers and using a short (10 min) etch in 50 % HF etch before lithography enables us to periodically pole wafers using a 200 V/mm, 300 ms long poling pulse. A 55 V/mm holding field was applied to prevent backswitching. Measured poling current suggests self-termination[19] occurs in VLT. The short HF etch before periodic poling enables a short (15 min) HF etch after poling to reveal domains. A full 2 inch wafer, poled with an 8 μm period for second harmonic generation (SHG) of 532 nm is shown in Fig. 9 with samples of $+z$ and $-z$ areas shown in the inset. Unpoled areas are the result of lithographic defects.

V. OPTICAL PROPERTIES

Optical properties that influence the utility of VLT, including measurements of the optical nonlinear coefficient, sensitivity to photorefractive damage, absorption, and laser-induced damage threshold are reported in this section. Since these properties may also be composition dependent, VLT will refer to near-stoichiometric lithium tantalate with a coercive field of approximately 100 V/mm unless otherwise stated.

A. Nonlinear coefficient

To measure the nonlinear coefficient of these materials, Maker fringe measurements[25] of the d_{33} coefficient of congruent lithium niobate, CLT, SLT prepared by double-crucible Czochralski growth from Oxide Corporation, and VLT were performed. Figure 10 shows a typical Maker fringe measurement for VLT, using 100 mW of 1064 nm single-frequency radiation and a beam size of 40×30 μm ($1/e^2$-intensity radius) at room temperature. The results are normalized to congruent lithium niobate and are tabulated in

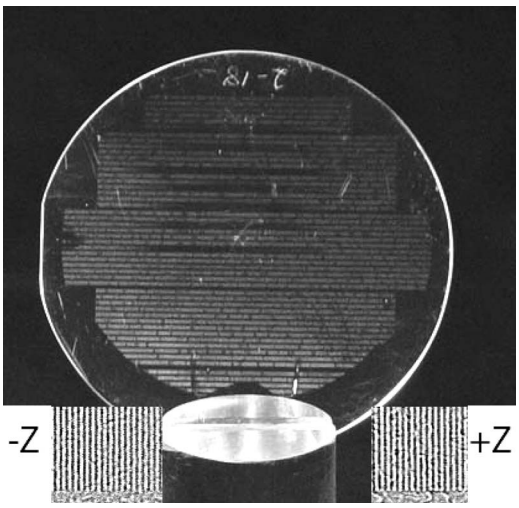

FIG. 9. A 2 inch SLT wafer (202–18) poled with an 8 μm period. Etched +Z and –Z faces are shown in the inset.

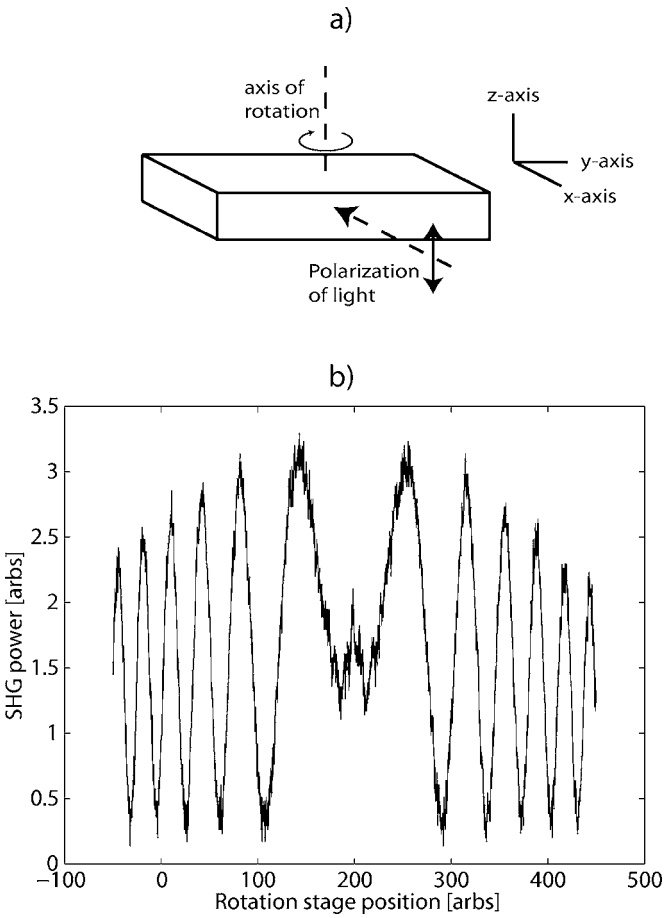

FIG. 10. (a) Crystal orientation and polarization of input light for the Maker fringe measurement of d_{33}. (b) A typical Maker fringe measurement of the d_{33} coefficient of VLT.

TABLE I. Maker fringe measurements of various crystals.

Sample	Nonlinear coefficient $d_{33,X}/(d_{33,CLN})$
Congruent LN	1
Congruent LT	0.67±0.05
Double crucible Czochralski SLT	0.70±0.05
VLT	0.67±0.05

Table I. All forms of LT show no significant difference in nonlinear coefficient to an accuracy of 5 %. This result does not agree with Ref. 26, which finds an increase of 15 % in the nonlinear optic coefficient of SLT. The origin of the discrepancy between Ref. 26 and these measurements is unclear.

B. Photorefraction

Historically, the limiting factors that have prevented high-power visible-light generation at near-room temperatures in ferroelectrics like LN and LT have been PRD and GRIIRA. These two effects are reduced as the density of intrinsic defects are reduced in stoichiometric and Mg-doped crystals. It has been shown that the coercive field (E_c) is proportional to the deviation of the composition from stoichiometry and thus with the density of intrinsic defects which cause PRD and GRIIRA.[9,14]

The correlation can be explained by examining the space-charge fields induced by the balance of photogalvanic and drift currents.[27] Consider a simplified (linear, one-dimensional) constitutive relation for charge transport in the crystal,

$$\mathbf{J} = \sigma\mathbf{E} + \kappa I\hat{\mathbf{z}}, \tag{2}$$

where $\mathbf{J}$ is the current density in the crystal, σ is the conductivity, $\mathbf{E}$ is the space-charge field in the medium, κI is the photogalvanic response to an optical intensity I, and $\hat{\mathbf{z}}$ is a unit vector along the ferroelectric axis. The conductivity is composed of both a dark conductivity and an intensity-dependent photoconductivity such that

$$\sigma = \sigma_{\text{dark}} + \sigma_{\text{ph}}(I). \tag{3}$$

In steady-state, i.e., $\mathbf{J}=0$, a steady-state electric field will exist in the crystal given by

$$\mathbf{E} = \frac{\kappa}{\sigma_{\text{dark}} + \sigma_{\text{ph}}(I)} I\hat{\mathbf{z}}. \tag{4}$$

At high intensity, the bulk conductivity will be dominated by the photoconductivity, which can be taken as linear in the intensity, i.e., $\sigma_{\text{ph}}=\beta I$. Thus, the steady-state electric field can be characterized by a saturated space-charge field, $\mathbf{E}_{\text{SC}} \rightarrow \kappa/\beta\hat{\mathbf{z}}$.[28] This saturated space-charge field is a measure of the field induced by the photogalvanic current, and is typical of the largest fields encountered even in more realistic three-dimensional geometries. Since the photorefractive index change is created through the combination of saturated space-charge field and the electro-optic effect, materials with smaller saturated space-charge fields will tend to be less sensitive to photorefractive damage.

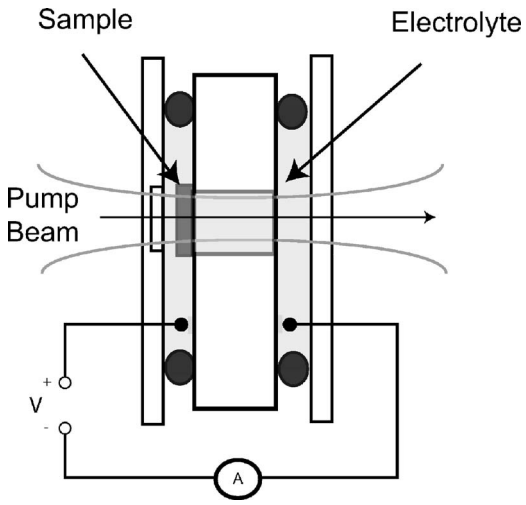

FIG. 11. Experimental diagram of apparatus for measurement of photoconductivity and photogalvanic coefficients. A probe beam is focused through the sample, and the photogalvanic and photoconductive currents are measured in a picoammeter. The sample is mounted on an insulating frame and contacted with liquid electrolyte contacts.

Reducing the lithium deficiency found in congruently melting crystals can decrease $\mathbf{E}_{\text{SC}}$ by increasing the photoconductivity. In the simplest model of conduction in these crystals, the conductivity is proportional to the carrier lifetime in the medium, which should be inversely proportional to the total number of deep traps in the crystal. By reducing the large defect density resulting from the nonstoichiometry of the congruent-composition crystals, one would expect, assuming the deep traps are associated with the stoichiometric defects, the conductivity to increase by orders of magnitude for a given charge generation rate in near-stoichiometric crystals; thus, the sensitivity to photorefractive damage would also decrease proportionately.

To characterize the transport properties that influence the saturated space-charge field in VLT, we measured the photoconductive and photogalvanic currents for a given light intensity and applied voltage. Use of a focused laser beam is necessary to reach optical intensities typical of frequency conversion interactions. To avoid pyroelectric currents resulting from heating due to absorption of the focused pump in conventional electrodes, we used a modified liquid-electrolyte, electric-field-poling cell illustrated in Fig. 11. The probe beam was focused through a quartz window to illuminate the sample. A picoammeter was used to measure the photoconductive and photogalvanic coefficients. The saturated space-charge field is the ratio of the photogalvanic coefficient to photoconductive coefficient.[1,8,9]

With 0.5 W of 514.5-nm radiation focused to a 35 μm spot ($1/e^2$-intensity radius), photogalvanic and photoconductive coefficients were measured for VLT at room temperature for samples fabricated with various VTE processing times shown in Table II.

From these measurements, one can estimate the maximum length useful for frequency conversion when limited by

TABLE II. Photorefractive properties of various VLT samples.

Sample name	VTE time at1360 °C (h)	Coercive field (V/mm)	Photogalvanic coefficient (pA/W)	Photoconductive coefficient [pS/(W cm)]	Saturated space charge field (V/cm)	$L_{\pi/10}$ (cm)
CLT	0	21 000	4.2[a]	0.003[a]	1270±300 [a]	0.13
17C	12	260	3.7±0.6	0.13±0.05	43±26	4.0
18B	18	170	8.6±1.1	0.33±0.19	32±20	5.3
147D	160	100	2.4±0.2	0.22±0.24	10±8	17

[a]Reference 9.

photorefraction. Photorefraction causes a negative lens which in turn causes the interacting beams to fan out, reducing beam quality and limiting nonlinear-device performance. The useful length for frequency conversion can be estimated by determining the length where the accumulated photorefractively induced phase shift reaches approximately $\pi/10$ for extraordinary polarized radiation and is given by

$$L_{\pi/10} = \frac{\lambda}{10 r_{33} n^3 E_{SC}}. \quad (5)$$

Here, $L_{\pi/10}$ is the useful length, λ is the wavelength, r_{33} is the electro-optic coefficient, n is the refractive index, and E_{SC} is the saturated space charge. In lithium tantalate at 532 nm, taking $r_{33} \approx 30$ pm/V and $n \approx 2.2$, this length is approximately given by

$$L_{\pi/10} \approx \frac{1000\lambda}{3E_{SC}} \approx \frac{170}{E_{SC}},$$

where $L_{\pi/10}$ is given in cm, λ is given in μm, and E_{SC} is given in V/cm. Considering the measured values, it is easy to understand why congruent lithium tantalate does not perform well at room temperature. The measurements of the transport properties listed in Table II show a 100-fold reduction of the saturated space-charge field in VLT compared to its congruent-composition counterpart. Photorefraction should not impose a limitation on conversion efficiency, since $L_{\pi/10}$ exceeds typical crystal lengths used in practical systems.

C. Absorptivity

In the absence of photorefraction, absorption in nonlinear materials ultimately sets the average-power-handling limit.[29,30] This absorption can arise either from extrinsic impurities, native defects, or intrinsic interband or multiphonon absorption. To measure the absorption in VLT, several measurement tools and experimental techniques were employed. Near the ultraviolet band edge, a Cary 500 spectrophotometer and a SOPRA spectroscopic ellipsometer (in transmission mode) were used to characterize the absorption for both the ordinary and extraordinary waves. In the visible and near-infrared, photothermal common-path interferometry[31] was used to measure both the absorption and any induced infrared absorption for various wavelengths. We define an induced infrared absorption as the increase of the infrared absorption caused by the presence of another wavelength. Finally, a Fourier transform infrared (FTIR) spectrometer was used to probe the absorption of the ordinary wave in the mid-infrared.

1. Ultraviolet absorption

To measure the ordinary polarized ultraviolet absorption of VLT, a Cary 500 spectrophotometer was used to measure the transmission of both CLT and VLT samples of thickness 0.2, 0.5, and 1 mm. The absorptivity was then calculated from the transmission spectra. The maximum thickness of VTE samples limited the sensitivity of the absorption to 0.1 cm^{-1}. To measure the extraordinary wave, a SOPRA spectroscopic ellipsometer aligned in transmission mode was used to measure transmission spectra of end-face-polished VLT samples of lengths 7, 10, and 20 mm. The maximum length of measured VTE samples and transmission uncertainty limited the sensitivity to approximately 0.05 cm^{-1}. Ordinary-wave absorptivity was also measured with the spectroscopic ellipsometer and was in good agreement with Cary 500 spectrophotometric data. Absorptivity of both VLT and CLT is shown in Fig. 12. These measurements agree with previous measurements on similar VLT and CLT of varying Fe^{2+} and Cr^{2+} concentrations.[32] It is important to note that these measurements are performed at low intensities and may not be exactly representative of what one would measure at laser intensities seen in frequency conversion experiments. It should also be noted that Ref. 33 characterized the composition of similar VLT samples via UV absorption edge to an accuracy of ±0.05 mol %. Using the wavelengths where the sample exhibits 20 and 50 cm^{-1} of ordinary-wave absorptivity, one can estimate the sample has a composition of 49.97 and 49.96 mol %, respectively. This estimation

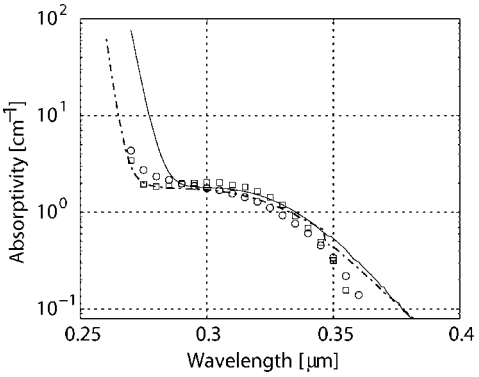

FIG. 12. Ordinary and extraordinary absorptivities for both CLT and VLT. CLT ordinary-wave absorptivity measured on the Cary 500 spectrophotometer is shown as the solid curve. VLT ordinary-wave absorptivity measured on the Cary 500 spectrophotometer is shown as the dashed curve. Circles and squares represent extraordinary-wave and ordinary-wave VLT absorptivity measured on the ellipsometer.

TABLE III. Absorptivity of VLT samples at various wavelengths.

Wavelength (nm)	O-wave absorptivity (%/cm)	E-wave absorptivity (%/cm)	Induced 1064-nm absorption[a] [%/(W cm)]
457	1.0–1.7	0.15–0.35	N/A
488	0.12–0.22	0.10–0.20	0.015–0.06
514.5	0.04–0.08	0.06–0.12	0.007–0.035
532	0.04–0.12	0.04–0.12	(0.05)-0[b]
808	0.01–0.02	0.00–0.01	N/A
1064	0.02–0.07	0.01–0.04	N/A

[a]The induced 1064-nm absorption is the measured increase in 1064 nm absorption due to the simultaneous illumination of the same volume with 488, 514, and 532 nm radiation.
[b]Parentheses indicate induced bleaching effect was measured.

agrees with the estimation of the composition via the ferroelectric coercive field method within the measurement error.

2. Visible and near-infrared absorption

In the visible and near-infrared, absorption in VLT and in CLT is too small to be measured by simple spectrophotometry. Photothermal common-path inteferometry[31] is a very sensitive technique which can measure absorptivities as low as 10^{-6} cm^{-1}. Using 457, 488, 514.5, 532, 808, and 1064 nm radiation, the absorptivity of VLT was probed as a function of polarization and position. Each beam was focused to a 40 μm spot ($1/e^2$-intensity radius) inside the crystal. The absorptivity was calculated by detecting the thermo-optic phase shift induced on a 633 nm probe beam. This same apparatus allows us to measure green-induced infrared absorption (GRIIRA).[32] Using a coaligned beam of 532 nm radiation, we can simultaneously illuminate the same volume of crystal with the 1064 and 532 nm radiation. This allows us to measure the change in absorption of the 1064 nm radiation with and without the 532 nm radiation. This change in absorption is the green-induced infrared absorption (GRIIRA). Although, the mechanism responsible for GRIIRA is unknown, the sensitivity to GRIIRA has been correlated with the number of antisite tantalum defects and thus the crystal stoichiometry. Previously, GRIIRA measurements using 514.5 nm radiation showed a 100-fold reduction in similarly fabricated VLT when compared to CLT.[9] Here, the induced 1064 nm extraordinary-wave absorption caused by the presence of extraordinary-polarized and coaligned 488, 514.5, and 532-nm radiation has been measured. Table III shows the results of these measurements.

CLT was also measured at 1064 and 532 nm and had absorptivities from 0.05–0.1 %/cm and 0.28–0.4 %/cm, respectively. Absorption in VLT varied in the plane of the sample. Variations could arise from either inhomogeneous distribution of defects or an inhomogeneous distribution of oxidation states of homogeneously distributed defects. Chemical reduction during either VTE or uniform poling that was not removed during the post-uniform-poling anneal could have introduced this inhomogeneity. Transient behavior similar to effects discussed in Ref. 32 were observed; however, only steady-state, cw absorption measurements are listed. The wavelength and polarization dependence of the absorption is consistent with absorption of Fe^{2+} impurities.[34,35]

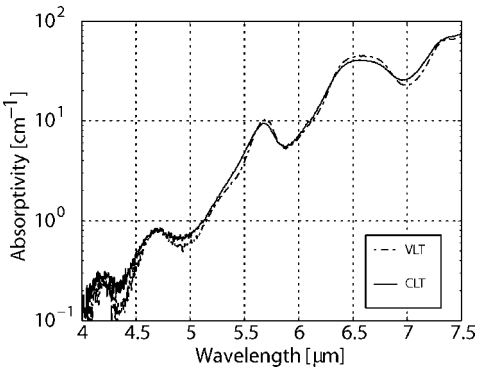

FIG. 13. Ordinary-wave absorptivities for both congruent LT (solid) and VLT (dashed) in the mid-infrared.

3. Mid-infrared absorption

To measure the mid-infrared absorptivity, a BioRad FTS-40 FTIR spectrometer was used. CLT and VLT samples of 0.2, 0.5, and 1 mm thicknesses were measured along the ordinary axis. Transmission of each sample was measured and the absorption was calculated. Figure 13 shows both these spectra.

Change in the ordinary-wave absorptivity near the 2.9 μm absorption band of OH^- was also measured. The absorption peak of VLT is shifted and is substantially narrower for VLT than CLT as shown in Fig. 14, which is consistent with past measurements.[36] The height of this peak varies with the VTE-process-atmospheric conditions. In lithium niobate, the OH^- absorption of both congruent and near-stoichiometric compositions have been measured and are similar to those in CLT and SLT, respectively. The narrowing of the OH^- absorptivity spectrum has been attributed to the removal of lithium vacancies and niobium antisite defects which modify the stretch-mode vibrational frequency.[37] Similar arguments would also explain the change in the OH^- absorption in VLT.

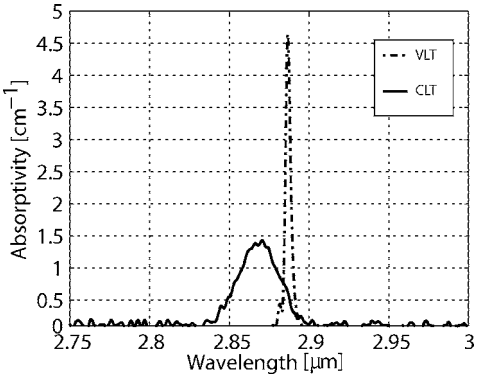

FIG. 14. Ordinary-wave OH^- absorptivities of congruent LT (solid) and VLT (dashed).

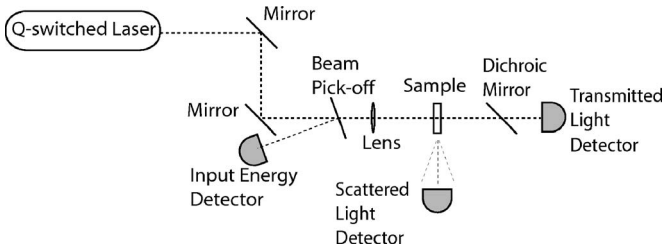

FIG. 15. Diagram of damage threshold measurement setup.

D. Optical damage threshold

For high energy pulses, surface or bulk optical damage will often set the limit for high peak power operation. To measure this effect, 3 mm long, uncoated samples of congruent lithium niobate, CLT, and VLT were polished and cleaned. A 12 ns pulsewidth, Q-switched, 2.4 mJ, 10 Hz-repetition-rate, multilongitudinal mode, single-transverse mode, 1064 nm Nd:YAG laser was loosely focused to a 55 μm spot ($1/e^2$-intensity radius) in the crystal. The length of 3 mm was chosen to avoid damage arising from self-focusing effects. Detectors were placed to monitor the input energy, the crystal transmission, and the scattered radiation. The experimental setup is shown in Fig. 15. The dichroic mirror was used to reject any stray second harmonic generation that could corrupt the measurement. By slowly increasing the input energy and monitoring the correlation of damage to crystal transmission and scattered radiation, statistics about multishot, laser-annealed damage probabilities as a function of input energy were collected. We defined the damage fluence as the largest fluence before crystal transmission began to decline, which was correlated with a steplike increase in scattering. The typical number of pulses incident on one location before damage occurred was approximately 200. Damage statistics are plotted in Fig. 16 with the number of test spots (N) for each sample indicated.

Measured damage fluence thresholds for congruent lithium niobate, CLT, and VLT are 2.3, 7.3, and 7.3 J/cm^2, respectively for a 55 μm radius. The damage threshold was measured by extrapolating the Weibull distribution back to zero probability. For all congruent lithium niobate samples surface damage was the predominant damage mechanism; however, for both CLT and VLT all samples damaged in the bulk before the surface. The CLT and VLT samples were all taken from different substrates. It is interesting to note that the two samples of CLT and VLT had widely different defect densities, and some volumes of LT did not damage at even the highest input energies. This suggests that both the defect itself and the concentration of bulk damaging defects in LT are determined by the growth of the original LT substrates.

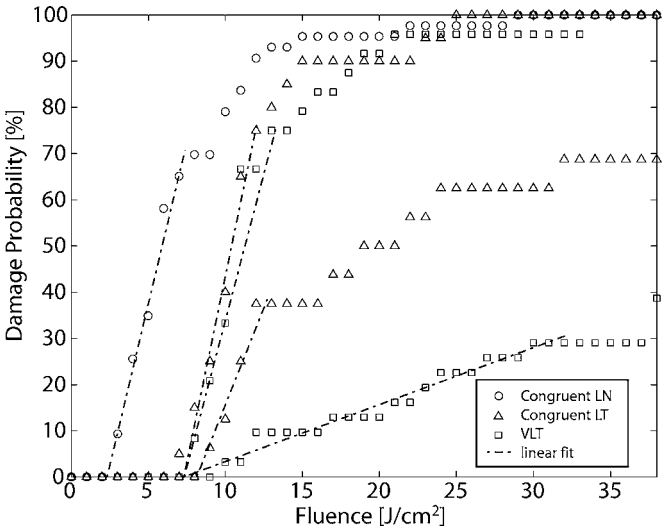

FIG. 16. Damage probabilities for congruent lithium niobate (circles, $N=43$) and two samples of both CLT (triangles, $N=20$, 16) and VLT (squares, $N=31$, 24).

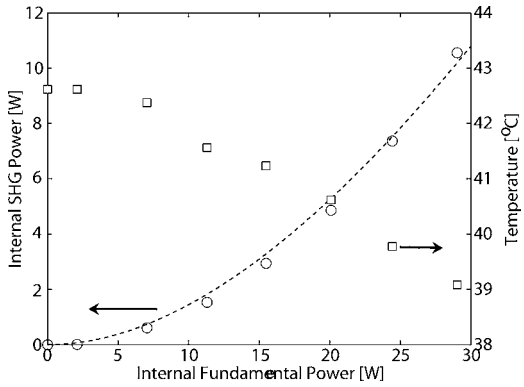

FIG. 17. Internal SHG power (circles) and optimum controller set-point temperature (squares) vs internal 1064 nm power. The dotted line is a quadratic fit to the internal SHG power as a function of input fundamental power.

VI. NONLINEAR DEVICE PERFORMANCE

To demonstrate the utility of full 2 inch wafer processing of VLT, nonlinear devices were fabricated from the wafer shown in Fig. 9. An uncoated, 4 cm long, 8 μm period device was used to generate the second harmonic of the output of a cw, 36 W, 4-stage master-oscillator-power-amplifier 1064 nm Nd:YAG source. The source had an M^2 value of 1.2 at 36 W and was focused to a 40 μm spot ($1/e^2$-intensity radius) into the crystal. The 4 cm long crystal generated 10.5 W of 532 nm SHG internally at the maximum pump power of 29 W internal and shows no signs of photorefractive damage or absorption limitations as shown in Fig. 17. Also shown in Fig. 17 is the optimum set point of the temperature controller. The linear decrease in optimal set point suggests that linear absorption of the fundamental dominates this change. A temperature tuning curve at maximum pump power was measured and is in good agreement with theoretical expectations for a 4 cm long device and the experimental focusing conditions as shown in Fig. 18. The M^2 value of the SHG radiation was measured to be 1.13 at 10.5 W of 532 nm radiation. The low-power, normalized efficiency of 0.4 %/(W cm) is approximately a factor of 2 smaller than ideal results for the focusing conditions. Results shown in Fig. 18 indicate that nonuniform composition (as measured in Sec. IV A) and thermal self-heating do not significantly affect device performance; thus, nonideal poling duty cycle appears to be the most likely source of this discrepancy. Fur-

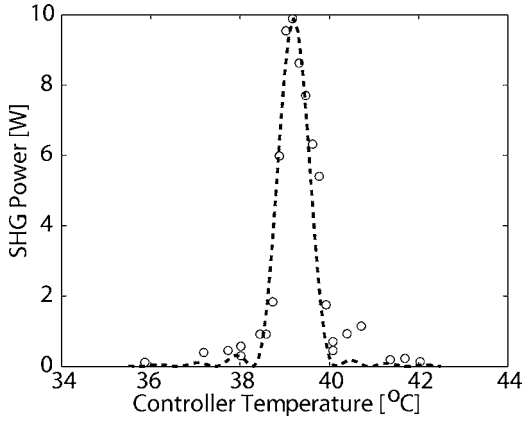

FIG. 18. SHG power vs temperature controller set point. The dotted line is the theoretical temperature tuning curve for the experimental focusing conditions.

ther improvements in periodic poling and lithography will improve overall nonlinear device performance.

From nonlinear measurements, it is likely that the maximum CW SHG power will be limited by the thermal dephasing which results from absorption of the 1064 nm radiation. Using a value of 8 W/(mK) taken from Ref. 5 as an approximate value for the thermal conductivity, a 0.5 cm crystal length, and including average values for absorption and induced 1064 nm absorptivity of 0.1 %/cm and 0.017 %/(W cm), one can estimate the maximum cw power at 200 W as in Ref. 29. This maximum could be increased by reducing the absorption in VLT crystals. Reducing the absorption would require either reducing the extrinsic impurity concentration during the growth process or improving the VTE or poling process to change the charge state of the existing defects so they do not absorb in the wavelength band of interest.

VII. CONCLUSION

The VTE process is an alternative to direct melt growth for producing photorefractive-damage-resistant SLT. Important optical properties pertaining to the limiting processes of nonlinear frequency conversion of SLT fabricated by VTE have been measured. The impact of VTE processing variations on the ferroelectric properties of VLT have been discussed. Periodic poling of full 2 inch wafers was shown and devices fabricated from these wafers generated 10 W of cw 532 nm radiation by SHG. This result has been achieved through the dramatic reductions of both PRD and 532 nm absorption in VLT. Estimates from absorption measurements suggest maximum cw power handling of approximately 200 W is possible in this material. It is clear that small-aperture (1 mm) bulk devices are readily achievable via the VTE process. Further work may extend these small-aperture devices to large-aperture devices for scaling to higher average and peak powers. Investigating the effects of various channel waveguide fabrication techniques on the photorefractive damage and absorption properties of VLT is also of interest.

ACKNOWLEDGMENTS

This research has been funded through the support of the Defense Advanced Research Projects Agency under Grant DAAD19–02–1-0184; the Air Force Office of Scientific Research under Grants FA9550–04–1-0465, FA9550–05–1-0184, and F49620–02–1-0240; Sony Corporation in Stanford Collaboration Agreement No. 30091; and the UCSC, Center for Adaptive Optics Subcontract S0159397. We acknowledge the support of Crystal Technologies Inc., Trek, Inc., and Lightwave Electronics Inc.

[1] M. Jazbinšek, M. Zgonik, S. Takekawa, M. Nakamura, K. Kitamura, and H. Hatano, Appl. Phys. B: Lasers Opt. **75**, 891 (2002).
[2] Y. Furukawa, K. Kitamura, A. Alexandrovski, R. K. Route, M. M. Fejer, and G. Foulon, Appl. Phys. Lett. **78**, 1970 (2001).
[3] Y. Furukawa, K. Kitamura, S. Takekawa, K. Niwa, and H. Hatano, Opt. Lett. **23**, 1892 (1998).
[4] A. G. Getman, S. V. Popov, and J. R. Taylor, Appl. Phys. Lett. **85**, 3026 (2004).
[5] N. E. Yu, S. Kurimura, Y. Nomura, and K. Kitamura, Jpn. J. Appl. Phys., Part 2 **43**, L1265 (2004).
[6] Y. Furukawa, K. Kitamura, E. Suzuki, and K. Niwa, J. Cryst. Growth **197**, 889 (1999).
[7] J. Shackelford and R. L. Holman, J. Appl. Phys. **46**, 1429 (1975).
[8] F. Holtmann, J. Imbrock, C. Baumer, H. Hesse, E. Kratzig, and D. Kip, J. Appl. Phys. **96**, 7455 (2004).
[9] M. Katz, R. K. Route, D. S. Hum, K. R. Parameswaran, G. D. Miller, and M. M. Fejer, Opt. Lett. **29**, 1775 (2004).
[10] M. Lines and A. Glass, *Principles and Applications of Ferroelectrics and Related Materials* (Oxford University Press, Oxford, 2001).
[11] P. F. Bordui, R. G. Norwood, C. D. Bird, and J. T. Carella, J. Appl. Phys. **78**, 4647 (1995).
[12] S. Kim, V. Gopalan, K. Kitamura, and Y. Furukawa, J. Appl. Phys. **90**, 2949 (2001).
[13] H. Guenther, R. Macfarlane, Y. Furukawa, K. Kitamura, and R. Neurgaonkar, Appl. Opt. **37**, 7611 (1998).
[14] L. Tian, V. Gopalan, and L. Galambos, Appl. Phys. Lett. **85**, 4445 (2004).
[15] B. T. Matthias and J. Remeika, Phys. Rev. **76**, 1886 (1949).
[16] R. L. Barns and J. R. Carruthers, J. Appl. Crystallogr. **3**, 395 (1970).
[17] A. A. Ballman, H. Levinstein, C. Capio, and H. Brown, J. Am. Ceram. Soc. **50**, 657 (1967).
[18] R. L. Holman and R. M. Fulrath, J. Appl. Phys. **44**, 5227 (1973).
[19] K. Nakamura, J. Kurz, K. Parameswaran, and M. M. Fejer, J. Appl. Phys. **91**, 4528 (2002).
[20] N. E. Yu, S. Kurimura, Y. Nomura, M. Nakamura, K. Kitamura, J. Sakuma, Y. Otani, and A. Shiratori, Appl. Phys. Lett. **84**, 1662 (2004).
[21] V. Y. Shur, A. I. Lobov, A. G. Shur, S. Kurimura, Y. Nomura, K. Terabe, X. Y. Liu, and K. Kitamura, Appl. Phys. Lett. **87**, 022905 (2005).
[22] G. D. Miller, R. G. Batchko, M. M. Fejer, and R. L. Byer, Proc. SPIE **2700**, 34 (1996).
[23] V. Y. Shur, E. L. Rumyantsev, E. V. Nikolaeva, E. I. Shishkin, D. V. Fursov, R. G. Batchko, L. A. Eyres, M. M. Fejer, and R. L. Byer, Appl. Phys. Lett. **76**, 143 (2000).
[24] J. H. Ro and M. Cha, Appl. Phys. Lett. **77**, 2391 (2000).
[25] W. N. Herman and L. M. Hayden, J. Opt. Soc. Am. B **12**, 416 (1995).
[26] S. M. Kostritskii, P. Bourson, M. Aillerie, M. D. Fontana, and D. Kip, Appl. Phys. B: Lasers Opt. **82**, 423 (2006).
[27] A. M. Glass, D. V. D. Linde, D. H. Auston, and T. J. Negran, J. Electron. Mater. **4**, 915 (1975).
[28] P. Gunter and J.-P. Huignard, *Photorefractive Materials and Their Applications* (Springer, Berlin, 1988).
[29] P. Blau, S. Pearl, A. Englander, A. Bruner, and D. Eger, Proc. SPIE **4972**, 34 (2003).
[30] P. F. Bordui and M. M. Fejer, Annu. Rev. Mater. Sci. **23**, 321 (1993).
[31] A. L. Alexandrovski, M. M. Fejer, R. P. Route, and R. L. Byer, in Pacific Rim Conference on Lasers and Electro-Optics, CLEO-Technical Digest, pp. 320–321 (2000).
[32] A. L. Alexandrovski, G. Foulon, L. E. Myers, R. K. Route, and M. M. Fejer, Proc. SPIE **3610**, 44 (1999).
[33] C. Bäumer, C. David, A. Tunyagi, K. Betzler, H. Hesse, E. Kratzig, and M. Wohlecke, J. Appl. Phys. **93**, 3102 (2003).

[34]H. Kurz, E. Kratzig, W. Keune, H. Engelmann, U. Gonser, B. Dishler, and A. Rauber, Appl. Phys. **12**, 355 (1977).
[35]S. A. Basun, D. R. Evans, T. J. Bunning, S. Guha, J. O. Barnes, G. Cook, and R. S. Meltzer, J. Appl. Phys. **92**, 7051 (2002).
[36]C. Baumer, C. David, K. Betzler, H. Hesse, K. Lengyel, L. Kovacs, and M. Wohlecke, Phys. Status Solidi A **201**, R13 (2004).
[37]Y. Kong, W. Zhang, X. Chen, J. Xu, and G. Zhang, J. Phys.: Condens. Matter **11**, 2139 (1999).